AIAA-2002-1456

FINITE ELEMENT ANALYSIS OF WRINKLED MEMBRANE STRUCTURES FOR SUNSHIELD APPLICATIONS

John D. Johnston
NASA Goddard Space Flight Center, Greenbelt, MD

Abstract

The deployable sunshield is an example of a gossamer structure envisioned for use on future space telescopes. The basic structure consists of multiple layers of pre-tensioned, thin-film membranes supported by deployable booms. The prediction and verification of sunshield dynamics has been identified as an area in need of technology development due to the difficulties inherent in predicting nonlinear structural behavior of the membranes and because of the challenges involved in ground testing of the full-scale structure. This paper describes a finite element analysis of a subscale sunshield that has been subjected to ground testing in support of the Next Generation Space Telescope (NGST) program. The analysis utilizes a nonlinear material model that accounts for wrinkling of the membranes. Results are presented from a nonlinear static preloading analysis and subsequent dynamics analyses to illustrate baseline sunshield structural characteristics. Studies are then described which provide further insight into the effect of membrane preload on sunshield dynamics and the performance of different membrane modeling techniques. Lastly, a comparison of analytical predictions and ground test results is presented.

Introduction

Future large-aperture space telescopes such as the NGST will require lightweight, deployable sunshields. Sunshields (also referred to variously as solar shades, thermal shields, and light shields) provide passive cooling and/or stray light control for observatory optics and instruments.[1] A conceptual design for the NGST observatory, referred to as the 'yardstick' concept, was developed by NASA to establish a reference design for the mission and to identify areas in need of technology development.[2] The 'yardstick' sunshield, Fig. 1(a), consists of multiple layers of pre-tensioned, thin-film membranes that are supported by deployable booms. The structural dynamics of the sunshield are a concern due to the telescope's strict line-of-site pointing requirements. Structural analysis techniques must accurately characterize sunshield dynamics to ensure that they will be attenuated by the observatory's attitude control system (ACS) and vibration isolation systems such that they will not impair observatory performance.

To mitigate risks associated with sunshield dynamics, a program of analysis and ground testing was undertaken by the NASA NGST team. The focus of these efforts is a subscale model of the NGST 'yardstick' sunshield, Fig. 1(b).[3-6] The main components of the sunshield test article are a central mounting block, four support tubes, and four thin-film membrane layers. The membranes are attached at the central block and at the tips of the support tubes. A ladder structure at the tube tips maintains the spacing between the membranes. The membranes are attached to the ladder via the constant force springs (CFS) that apply the preloads. The test article is 3.4 m (134 in) long by 1.52 m (60 in) wide and has a total mass of 5 kg (11 lb). A modal survey of the test article was completed in vacuum to gain insight into sunshield dynamics and to provide data for model correlation studies. The test setup consists of the sunshield test article, a test stand, an electrodynamic shaker, and the instrumentation suite. A schematic of the test setup is shown in Fig. 2. The test article is attached to the shaker armature at the central block and is subject to base motion excitation. The instrumentation suite for the tests consists of accelerometers, force gages, and a laser vibrometer. Tri-axial accelerometers are located at the tip of each tube, on the central block, and on the test stand. A force gage is located at the central block-shaker interface point. The laser vibrometer is used to measure the response of the outer membrane layer. Tests were completed with the sunshield in two orientations: short side down and long side down.

This paper describes new efforts to analyze the static and dynamic behavior of this sunshield. First, an overview of the membrane modeling techniques utilized to study the sunshield will be presented. A new finite element model that accounts for the effects of wrinkling via a nonlinear material model will then be described and results from a baseline analysis presented. Next, results from the new wrinkled membrane model will be compared with predictions from alternate finite element models. Then, a parameter study carried out to investigate the effects of varying the CFS preloads will be described. Lastly, a comparison between analytical predictions and ground test results will be presented.

Membrane Modeling Techniques

Structural modeling of sunshields is challenging due to the complicated behavior of the thin-film membrane layers. Thin-film membranes in a stress free state have negligible bending stiffness. Out-of-plane stiffness is obtained by applying in-plane tensile loads and must be properly accounted for in structural models. In the case of the NGST sunshield design considered here, the out-of-plane structural stiffness is derived from the tensile loading applied at the membrane corners by constant force springs. An important characteristic of membrane structural behavior is wrinkling. Structural (or stress) wrinkles are out-of-plane deformations that occur due to local buckling in regions of the membrane that develop compressive stresses. The details of the wrinkling are dependent upon both the loading and boundary conditions for the structure. Wrinkles must be adequately accounted for in sunshield models because their presence alters the in-plane stress distribution, and hence the differential stiffness of the structure.[7] Typically, the capabilities of commercially available finite element codes are inadequate to model thin-film membrane wrinkling behavior. Several approaches were investigated for modeling the behavior of the sunshield membranes, including: standard element formulations, the cable network method, and membrane elements in conjunction with a wrinkling material model.

Modeling the thin-film membrane layers using standard membrane or shell elements in the presence of compressive stresses can lead to inaccurate results because the in-plane stress distribution will not be represented properly, and there may be numerical problems during out-of-plane dynamics analyses. Shell elements were initially utilized to model the sunshield, but the normal modes analyses yielded spurious 'noise' modes which led to the investigation of alternative modeling techniques. The cable network method was developed specifically for modeling the dynamics of pre-tensioned, wrinkled membranes.[8] The approach is based on the Stein-Hedgepeth wrinkling theory where it is established that load transfer in wrinkled regions takes place along wrinkle lines. [9] In this approach, the membrane is meshed with a network of rod elements that is mapped to the wrinkle pattern of the structure. This technique is useful for determining the out-of-plane structural dynamic characteristics of wrinkled membrane structures; however, it is limited in that it requires knowledge of the wrinkle pattern to create the cable network. This method was previously been used to model the 1/10th scale NGST yardstick sunshield.[3-4] A more accurate representation of wrinkled membrane structural behavior can be obtained by using membrane finite elements in conjunction with a wrinkling (i.e. no-compression or tension field) material model.[10-13] In this approach, the state (wrinkled, slack, or taut) of each membrane element is assessed using a wrinkling criteria and the material properties are adjusted iteratively during the analysis to account for the behavior associated with the particular state of that element. The advantages of this method are that it can be used to accurately determine the in-plane stress state in the presence of wrinkling, as well as predict wrinkle characteristics including wrinkled region geometry and wrinkle directions. In the present study, the sunshield membranes are modeled using membrane elements in conjunction with a wrinkling material model.

Sunshield Analysis

A new structural analysis of the 1/10th scale NGST sunshield was performed using a wrinkling material model. The following sections describe the technique used to analyze the sunshield membranes, details of the overall finite element model, and results from a baseline analysis.

Analysis Technique

The analysis was performed using the commercially available finite element analysis program ABAQUS.[14] Sunshield structural response is predicted using a nonlinear static analysis that accounts for membrane wrinkling effects through use of a user defined material (UMAT) subroutine. The UMAT utilized here was developed by Adler.[10] In this approach, membrane element material properties are iteratively modified during the analysis to account for the effects of wrinkling and slackness. The analysis procedure is as follows. First, a finite element model of the structure is generated using membrane elements that are assigned the wrinkling material model. Next, a nonlinear static analysis of the structure is performed during which the state of each element (taut, slack, or wrinkled) is determined. A combined stress-strain criteria is used in the UMAT to determine the element states. Following the elements state determination, the stiffness matrix of each element is updated as follows. If the element state is taut, the stiffness matrix is unaltered. If the element state is slack, the stiffness matrix is set equal to zero. If the element state is wrinkled, the stiffness matrix is modified according to Stein-Hedgepeth wrinkling theory.[9] This theory predicts that the stress state in a wrinkled region of a membrane is uni-axial (positive major principal stress and zero minor principal stress) and wrinkles form in straight lines along the direction of the major principal stresses (load transfer in the wrinkled region is along these lines). Note that this theory predicts average strains and displacements in the wrinkled region, but not individual wrinkle details (such as wrinkle amplitude and wavelength).

Finite Element Model

The finite element model of the sunshield is shown in Fig. 3. The model includes four thin-film membrane layers, four aluminum support tubes and their associated tip hardware, and a central mounting block. The membranes are 1.27E-5 m (0.0005 in) thick kapton and are modeled using membrane elements which are assigned a wrinkling material model. Each of the four membrane corners has a catenary that is reinforced with a kevlar string and mylar tapes. The string is 5.08E-4 m (0.02 in) in diameter and is modeling using beam elements. The tapes are 2.54E-4 m (0.001 in) thick and are modeled using shell elements. The membranes are attached to the support tubes via a spreader bar and constant force spring (CFS) at each corner. The spreader bars are modeled using beam elements. The baseline CFS apply a preload of 1.425 N (0.32 lb) and are modeled using beam elements. Two additional CFS were considered: CFS2 = 2.848 N (0.64 lb) and CFS3 = 4.272 N (0.96 lb). The CFS forces are modeled using the ABAQUS *PRE-TENSION SECTION feature. This method is typically used to model fastener preloads. At the end of each tube is a ladder structure to which the CFS are attached. The ladder structures maintain the correct spacing between the membrane layers and are modeled with beam elements. An accelerometer was mounted on the end of each tube during ground testing. The total mass of the ladder, CFS, and accelerometer is represented by a concentrated mass element located at the tip of each support tube. The tip masses for each of the configurations are: CFS1 = 34.1 g, CFS2 = 29.6 g, and CFS3 = 32.2 g. The aluminum support tubes have a circular cross-section (radius = 0.007938 m, wall thickness = 0.001651 m) and are modeled using beam elements. The density of the tubes has been modified to account for the additional mass of the accelerometer cables used in the ground tests. The central block is represented using solid elements, with the connections between the tubes and the central block modeled using rigid elements.

The sunshield is supported at the central block. A bolt passes through the center of the block and attaches the model directly to the armature of the shaker for dynamic testing. A force gage (represented in the model by a stiff beam element) is located at the interface between the central block and the shaker armature. Two support conditions were evaluated: fixed support and shaker support. The fixed support condition was used for the baseline analysis and case studies, while the shaker support condition was used for simulating the ground tests. The fixed support model constrains the sunshield in all degrees of freedom (DOF 123456) at the attachment point of the test article to the shaker.

The shaker support case includes a 0.4 Hz rigid body translational mode of the sunshield/shaker armature in the z-direction observed in the ground tests. For the shaker support case, a simplified two node support model is included. One node is at the attachment point of the sunshield to the shaker, while the other node is constrained in all degrees of freedom. The nodes are connected by a rigid element with dependent DOF 12456 and an element with stiffness in DOF 3 selected to reproduce the 0.4 Hz rigid body mode. Previous studies demonstrated that it was necessary to model this support condition to provide representative analytical predictions for comparison with the test results.[4]

Baseline Analysis Results

The baseline analysis of the sunshield consists of a nonlinear static preloading analysis to determine the stresses and preloaded geometry subject to the CFS1 preloads in the absence of gravity loading, a modal analysis to determine natural frequencies and mode shapes, and finally a mode-based random response analysis to characterize the frequency domain response. The preloading analysis consists of two nonlinear static analysis steps. In the first step the membranes are subjected to an initial preload and constrained to undergo only in-plane deformations (required to remain flat). This is necessary to develop some initial out-of-plane stiffness in the membrane elements. In step 2 the out-of-plane constraints are removed and the full CFS preloads are applied leading the membranes to naturally develop the correct deformed configuration and wrinkled stress state. Figure 4 shows the initial undeformed shape and the final preloaded configuration for the sunshield. Figures 5(a)-(b) present contour plots of the major and minor principal stresses in the outermost membrane layer after preloading for the baseline case (CFS1= 1.425 N). The major principal stresses range from a peak of 1.26 MPa (180 psi) to a minimum of 0.02 MPa (3.3 psi) in the outer membrane layers and 1.09 MPa (160 psi) to 0.06 MPa (8.7 psi) in the inner membrane layers. The minor principal stresses range from a peak of 0.17 MPa (25 psi) to a minimum of 0 MPa (0 psi) in the outer membrane layers and 0.18 MPa (26 psi) to 0 MPa (0 psi) in the inner membrane layers. The differences in the stresses between the outer and inner membrane layers are due to the differing final geometries (the membranes are not co-planar, there is a small angular spread between layers). The wrinkled region in the outermost membrane layer is shown in Fig. 5(c) and is seen to encompass a majority of the membrane. Note that the predicted wrinkle regions for the inner membranes are slightly smaller than that of the outer membranes, and that the present analysis does not predict the presence of any slack regions in the membranes.

A modal analysis of the preloaded sunshield predicts 347 modes in the 0–10 Hz frequency range. The fundamental mode of the system has a frequency of 2.54 Hz and is a membrane mode involving twisting of the long side of the membranes about the y-axis. Significant sunshield modes were selected using modal effective mass (EFFM) in the RX direction as a selection criteria. This metric was used throughout the study to select the significant 'flexible' modes of the system since out-of-plane bending modes of the sunshield will have the greatest impact on telescope pointing. There are 31 modes having greater than 0.1% EFFM-RX. These modes account for 94% of the rigid body mass of the sunshield in the RX direction (the sum total % EFFM for all 347 modes is 96%). Mode 17 has the highest effective mass and involves the long support tube with participation from the long sides of the membranes. A random response analysis was performed to predict the response of the sunshield in the frequency domain. The excitation consisted of a base acceleration of 10 mg, rms in the z-direction over a frequency range of 0–10 Hz. The analysis included all modes having EFFM-RX > 0.1% (31 modes) and a value of 2% of critical damping assumed for all modes. Figure 6 presents the magnitude of the transfer functions between the input acceleration and the response at the tips of the long, medium, and short support tubes (acceleration transfer function magnitudes). There are several peaks in the long tube response. The largest peak corresponds to the frequency of the dominant mode identified in the modal analysis (mode 17). There are essentially two major peaks in the medium tube response at frequencies corresponding to modes 110 and 150. Table 1 presents a list of key system modes that were identified from the modal and random response analyses. Mode shape plots for these modes are presented Fig. 7 (note that the eigenvectors have been normalized such that the largest displacement entry in each vector is unity).

Table 1: Key system modes for baseline sunshield.

Mode #	F (Hz)	% EFFM	Notes
3	2.67	8.1	Long side of membranes (edge flapping)
17	3.37	15.6	Long tube / Long side of membranes
25	3.54	10.2	Long tube / Long side of membranes
110	5.52	5.0	Medium tube / Short side of membranes
150	6.28	8.4	Medium tube / Short side of membranes

Based on inspection of results from the modal and random response analyses, the sunshield modes were categorized into two broad groups. The first group are essentially local membrane modes and involve little or no participation from the support tubes. The lowest frequency modes of the system are membrane modes. Additionally, there are a number of higher-order membrane modes predicted by the modal analysis in the 3–6 Hz that involve little or no participation from the support tubes. The second group are membrane-tube interaction modes. These modes fall within frequency bandwidths surrounding the first mode of the long support tube (approximately 3–4 Hz) and the first mode of the medium length support tube (approximately 5–6 Hz). In general, the membrane tube interaction modes have much greater effective mass than the membrane modes.

Preload Effects Study

A parameter study was carried out to investigate the effects of varying the preload applied to the membranes by the CFS on the dynamic response of the sunshield. Three different CFS values were considered: CFS1=1.425 N (baseline), CFS2=2.848 N, and CFS3=4.272 N. As was the case with the baseline sunshield design, for each of these cases the corners of the membrane were loaded equally. The following analyses were completed for each case: nonlinear static preloading analysis, modal analysis, and random response analysis. The preloading analyses predict that the membrane stresses increase linearly with the increase in preload. The size and shape of the wrinkle regions in the membranes show little change. Modal analyses were completed for both the full sunshield and the sunshield support structure (i.e. sunshield without membranes). There are two significant modes of the support structure in the 0-10 Hz frequency range that correspond to bending modes of the long and medium length tubes. The frequencies of these modes vary between the three sunshield configurations due to: (1) changes in the CFS preloads (increasing the preload decreases the tube frequency) and (2) changes in the total mass of the tip hardware (increasing the tip mass decreases the tube frequency). The long tube mode frequencies for each case are: CFS1=3.54 Hz, CFS2=3.49 Hz, and CFS3=3.35 Hz. The medium tube mode frequencies for each case are: CFS1=5.84 Hz, CFS2=5.86 Hz, and CFS3=5.69 Hz. Modal analysis predictions for the full sunshield demonstrate that several aspects of system dynamics are altered by varying the preloads as summarized in Table 2.

Table 2: Summary of modal analysis predictions from preload effects study.

Parameter	CFS1	CFS2	CFS3
# of Modes	347	278	184
Total EFFM (%)	96	93	95
F_0 (Hz)	2.54	2.66	3.10
F_1 (Hz)	2.67	2.68	3.10
F_A (Hz)	2.54	2.66	3.12
F_B (Hz)	3.37	3.30	3.43

The number of modes identified in the 0-10 Hz frequency range decreased as the preload increased,

while the sum total effective mass remained unchanged. The frequencies and mode shapes of the complete sunshield were altered by the increase in preload. The frequency of the first mode (designated F_0 in Table 2) is seen to increase with increasing preload. The frequency of the first significant mode (having EFFM-RX > 1% and designated F_1 in Table 2) is also seen to increase with increasing preload. Node that these are not necessarily the same modes with frequency shifts, the modes shapes change significantly. Mode A involves twisting of the long side of the membranes about the y-axis. The frequency of this mode increased with increasing preload, while the mode shape remained approximately the same. Mode B is the mode with greatest effective mass and corresponds to a membrane-tube interaction mode near the frequency of the first bending mode of the long tube. The frequency of this mode is relatively unaffected by the increase in membrane preload, however the effective mass of this mode increases with increasing preload and the mode shape change significantly. Figure 8 presents mode shapes for mode B for each of the three CFS cases. In each case a central region of the long side of the membranes moves in-phase with the end of the long support tube, while regions along the edges move out-of-phase with the tube. Note that as the membrane preload increases, the size of the central region increases, while that of the edge regions decreases. Results from the random response analyses provide insight into the effects of preload on the frequency domain characteristics of the sunshield. Figure 9 presents plots of the acceleration transfer function magnitudes for the long and medium support tubes, while Table 3 summarizes the frequencies of the two largest peaks associated with the response at the tips of the long and medium support tubes. Note that the two largest peaks in response of the long tube bracket the frequency of the fundamental mode of the long tube without membranes for each configuration. Similar behavior is noted for the medium tube. Note that the frequency of the largest peak in the long tube response corresponds to the frequency of the mode with the greatest modal effective mass for each case. Inspection of the frequency response plots also shows that as the membrane preload increases, the number of significant sunshield modes decreases. Finally, it is noted that as the membrane preload increases, the peak response of the sunshield to a given input increases.

Table 3: Summary of random response analysis predictions from preload effects study.

Peak Response	Frequency (Hz)		
	CFS1	CFS2	CFS3
Long tube - Peak 1	3.37	3.30	3.43
Long tube - Peak 2	3.55	3.74	3.10
Medium tube - Peak 1	6.31	5.38	5.45
Medium tube - Peak 2	5.52	6.37	6.21

Membrane Modeling Technique Study

A study was completed to compare predictions for the baseline (CFS1) sunshield using the following three membrane modeling techniques: the current membrane element with wrinkling material model (referred to as the wrinkled membrane model in the following discussion), shell element, and cable network. The shell element model is identical to the wrinkled membrane model, except that the membrane elements with the wrinkling material model have been replaced with shell elements having isotropic material properties. The cable network sunshield model is described in detail in Ref. 4. Comparison of membrane stresses from the preloading analysis can only be made between the shell and wrinkled membrane models since the cable network modeling approach does not provide stress predictions. For the wrinkled membrane model, the major principal stresses range from 1.26 MPa (180 psi) to 0.02 MPa (3 psi) in the outer membrane layers, while with the shell element model the stresses range from 1.61 MPa (233 psi) to -0.01 MPa (-1 psi). For the wrinkled membrane model, the minor principal stresses range from 0.17 MPa (25 psi) to 0 MPa (0 psi) in the outer membrane layers, while with the shell element model the stresses range from 1.09 MPa (158 psi) to -1.09 MPa (-158 psi). The major difference between the results is the presence of both negative major and minor principal stresses in the shell element model predictions. Note that the negative major principal stresses predicted by the shell model correspond to a slack region that was not predicted by the wrinkled membrane model. Table 4 presents a summary of modal analysis results.

Table 4: Summary of modal analysis predictions from membrane modeling technique study.

Parameter	Wrinkled Membrane	Shell	Cable Network
# of Modes	347	156	103
Total EFFM (%)	96	96	95
F_0 (Hz)	2.54	1.41	2.50
F_1 (Hz)	2.67	3.10	2.50
F_A (Hz)	2.54	2.86	2.64
F_B (Hz)	3.37	3.59	3.61

The total number of modes predicted by each of the models varies significantly, but the total effective mass in the 0 – 10 Hz frequency range is approximately the same. The lowest frequency mode (designated F_0 in Table 4) is approximately the same for the wrinkled membrane and cable network models. The lowest frequency mode predicted by the shell model is a so-called noise mode wherein the mode shape involves seemingly random membranes motions.[10] The

frequency of the first significant mode (having EFFM > 1% and designated F_1 in Table 4) varies between the models, with the shell element model predicting the highest frequency. The mode shapes for each of these modes primarily involve the long side of the membranes with some participate from the long tube. The shell model mode shapes display some asymmetry while those predicted by the wrinkled membrane and cable network models are symmetric. The frequencies and mode shapes for mode A (involving twisting of the long side of the membranes about the y-axis) are similar for each of the models. The frequencies of the mode having the greatest effective mass (designated mode B in Table 5) are within 10%, however the effective mass and mode shapes varying significantly. Figure 10 presents mode shape contour plots from each of the models for mode B. The mode involves participation from both the long side of the membranes and the long support tube. In each case a central region near the end of the long side of the membranes moves in-phase with the tip of the tube. Each of the models also predicts a region of the membranes moving out-of-phase with the tip of the tube, however, the size and location of this region varies significantly from model to model. In general, there is considerable variation in the results predicted by the three sunshield models. Importantly, while the frequencies of the dominant system mode are similar, the effective mass and mode shapes predicted by the three approaches differ substantially.

Comparison with Ground Test Results

Ground testing of the one-tenth scale model NGST 'yardstick' concept sunshield was completed in July 2000 and December 2001 at NASA Goddard Space Flight Center. A detailed summary of the test setup and results is provided in Refs 5-6, 15. The ground tests identified approximately twelve sunshield modes in the 0 – 10 Hz frequency range for each sunshield configuration. The lowest frequency modes of the sunshield primarily involve the outer edges of the membranes with no participation from the support tubes. There are typically two dominant sunshield modes that involve significant interaction between the membranes and support tubes. The frequencies of these modes roughly correspond to the frequencies of the fundamental bending modes of the long and medium tubes. The remaining modes fall into two categories: membrane modes and membrane-tube interaction modes. The majority of the membrane modes occur in the 1 – 3 Hz frequency range (i.e. up to the frequency of the first membrane-tube mode) and exhibit little or no participation from the support tubes. These appear to be local modes often involving flapping of the membrane edges. There were also a few membrane modes in the > 3 Hz frequency range that exhibit higher order membrane motions that also exhibit little support tube participation. The membrane-tube interaction modes occur in the frequency range of 3 – 8 Hz and involve higher-order membrane modes and participation from the long and medium length support tubes.

The analysis of the ground tests included two modifications to the previously described analysis. First, the shaker support condition was utilized in order to account for the shaker armature mode observed in the tests. Second, gravity loading was included to provide predictions for both the long and short side down test configurations. Table 5 presents a comparison of analytical predictions and test results for the dominant system modes observed in the ground tests. Results are compared for both the sunshield support structure without membranes (Tubes-LSD/SSD) and each of the sunshield configurations tested in December 2001 (SS-CFS1-LSD, SS-CFS2-SSD, SS-CFS2-LSD, and SS-CFS3-LSD).[15] The LT mode indicates the dominant mode associated with the long support tube, while MT denotes that associated with the medium tube.

Table 5: Comparison of analytical predictions and ground test results for dominant sunshield modes.

Configuration	Mode	Analysis	Test	% Diff
Tubes-LSD	LT	3.77	3.63	-3.8
	MT	6.06	5.75	-5.4
Tubes-SSD	LT	3.71	3.43	-8.2
	MT	6.10	5.92	-3.1
SS-CFS1-LSD	LT	3.57	3.35	-6.6
	MT	5.51	5.51	0.0
SS-CFS1-SSD	LT	3.54	3.21	-10.3
	MT	6.36	5.83	-9.1
SS-CFS2-LSD	LT	3.22	3.22	0.0
	MT	6.44	5.57	-15.6
SS-CFS3-LSD	LT	3.55	3.21	-10.6
	MT	5.65	5.85	3.4

A quantitative comparison was made between the analytical predictions from the uncorrelated finite element model and coarse mode shapes obtained from the testing using modal assurance criteria (MAC) calculations between the eigenvectors. The results demonstrate that, in general, the analysis correctly predicts the dominant modes. The predicted frequencies of the support tubes (without the membranes) show differences with the test results ranging from 3% - 8% and the mode shape correlation was excellent. For the complete sunshield, the dominant system modes exhibited the best correlation. The predicted frequencies show differences with the test results ranging from 0% - 16% (average = 6%). The correlation was poor for the lowest frequency membrane modes. It is believed that this is due to three

factors: (1) in some cases the test modes exhibited significant asymmetries not present in the analytical predictions, (2) the analytical model does not predict any slack regions in the membrane while inspection of the test article during ground testing revealed that presence of regions along the outer edges of the membranes that appeared to be slack, and (3) the current analytical predictions show only small changes due to the inclusion of gravity effects that the ground tests showed to actually be significant. Figure 11 presents a comparison of the predicted and measured mode shapes for the dominant modes of the sunshield with the CFS1, CFS2, and CFS3 preloads in the long side down orientation. In general, the mode shapes agree well in a qualitative sense for both of these modes. Note that the test shapes exhibit asymmetries that are not evident in the predicted shapes.

Conclusions

A new analysis of a one-tenth scale NGST sunshield was completed using membrane elements in conjunction with a wrinkling material model to model the behavior of the thin-film membrane layers. Results from a baseline analysis and a membrane preload parameter study demonstrated key aspects of sunshield static and dynamic behavior. A comparison of predictions from sunshield models using three different membrane modeling techniques was completed. Significant differences were seen in the predictions from each of the models, indicating that efforts to analyze pretensioned, thin-film membrane structures should not rely on any single technique for the prediction of critical system performance characteristics. Finally, a comparison of analytical predictions and results from ground tests was presented. The wrinkled membrane sunshield model exhibited good correlation with test results for the dominant system modes.

References

1. Perrygo, C., "Solar Shades," *Gossamer Spacecraft: Membrane and Inflatable Structures Technology for Space Applications*, Progress in Astronautics and Aeronautics, Volume 191, Edited by Christopher M. Jenkins, 2001, pp. 503-526.

2. Bely, P.Y., Perrygo, C. and Burg, R., "NGST "Yardstick" Mission," NGST Monograph No. 1, July 1999, available at http://ngst.gsfc.nasa.gov.

3. Lienard, S., Johnston, J.D., Adams, M.L., Stanley, D., Alfano, J.P., Romanacci, P., "Analysis and Ground Testing for Validation of the Inflatable Sunshield in Space (ISIS) Experiment". *41st AIAA Structures, Structural Dynamics, and Materials Conference*, Atlanta, GA, April 2000, AIAA-2000-1638.

4. Johnston, J. and Lienard, S., "Modeling and Analysis of Structural Dynamics for a One-Tenth Scale Model NGST Sunshield", *42nd AIAA Structures, Structural Dynamics, and Materials Conference*, Seattle, WA, April 2001, AIAA-2001-1407.

5. Johnston, J., Lienard, S., Ross, B., and Smith, J., "Dynamic Testing of a One-Tenth Scale NGST Sunshield in a Vacuum Environment – Test Report," NASA Goddard Space Flight Center, March 2001, available at http://ngst.gsfc.nasa.gov.

6. Lienard, S., Johnston, J., Ross, B., and Smith, J., "Dynamic Testing of a Subscale Sunshield for the Next Generation Space Telescope (NGST)," *42nd AIAA Structures, Structural Dynamics, and Materials Conference*, Seattle, WA, April 2001, AIAA-2001-1268.

7. Fang, H.F and Lou, M.C., "Analytical Characterization of Space Inflatable Structures-An Overview," *40th AIAA Structures, Structural Dynamics, and Materials Conference*, St. Louis, MO, April 1999, AIAA-99-1272.

8. Adler, A.L., Mikulas, M.M., and Hedgepeth, J.M., "Static and Dynamic Analysis of Partially Wrinkled Membrane Structures," *41st AIAA Structures, Structural Dynamics, and Materials Conference*, Atlanta, GA, April 2000, AIAA-2000-1810.

9. Stein, M. and Hedgepeth, J.M., "Analysis of Partly Wrinkled Membranes," Langley Research Center, Langley Field, VA, NASA Technical Note D-813, July 1961.

10. Adler, A.L., "Finite Element Approaches for Static and Dynamic Analysis of Partially Wrinkled Membrane Structures," PhD Thesis, Department of Aerospace Engineering, University of Colorado, Boulder, CO, 2000.

11. Schur, W.W., "Development of a Practical Tension Field Material Model for Thin Films," *32nd Aerospace Sciences Meeting*, Reno, NV, AIAA-94-0636.

12. Wong, Y.W., "Analysis of Wrinkle Patterns in Prestressed Membrane Structures," Dissertation, University of Cambridge, Department of Engineering, August 2000.

13. Blandino, J.R., Johnston, J.D., and Dharamsi, U.K., "Corner Wrinkling of a Square Membrane due to Symmetric Mechanical Loads," submitted to *Journal of Spacecraft and Rockets*, July 2001.

14. ABAQUS /Standard User's Manual, Version 6.1, Hibbitt, Karlsson, & Sorensen, Inc., Pawtucket, RI, 2000.

15. Ross, B., Johnston, J., and Smith, J., "Parametric Study of the Effect of Membrane Tension on Sunshield Dynamics," *43rd AIAA Structures, Structural Dynamics, and Materials Conference*, Denver, CO, April 2002, AIAA-2002-1459.

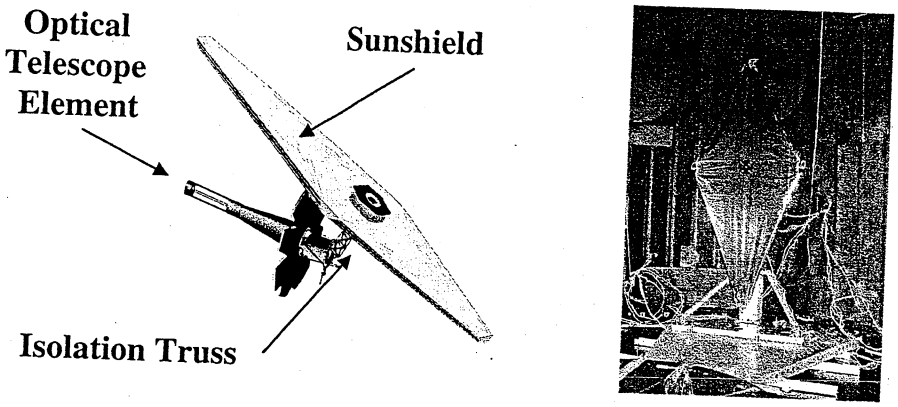

Figure 1: NASA 'yardstick' concept for the Next Generation Space Telescope (NGST): (a) schematic of observatory and (b) photograph of 1/10th scale model sunshield during ground testing.

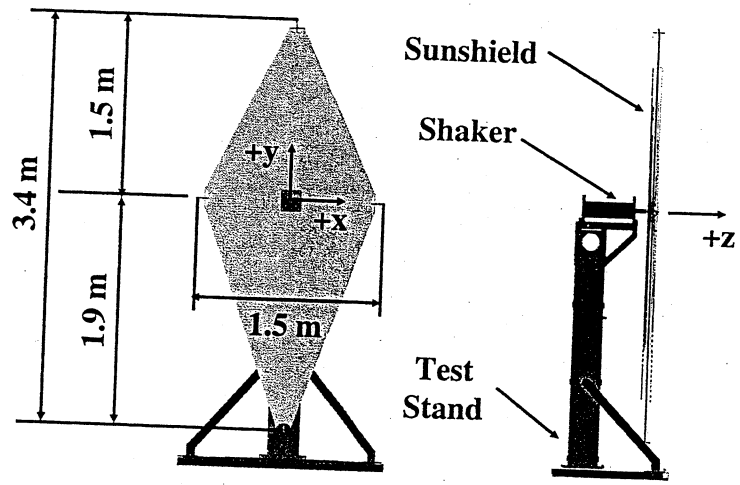

Figure 2: Schematic of ground test setup with sunshield in the long side down orientation.

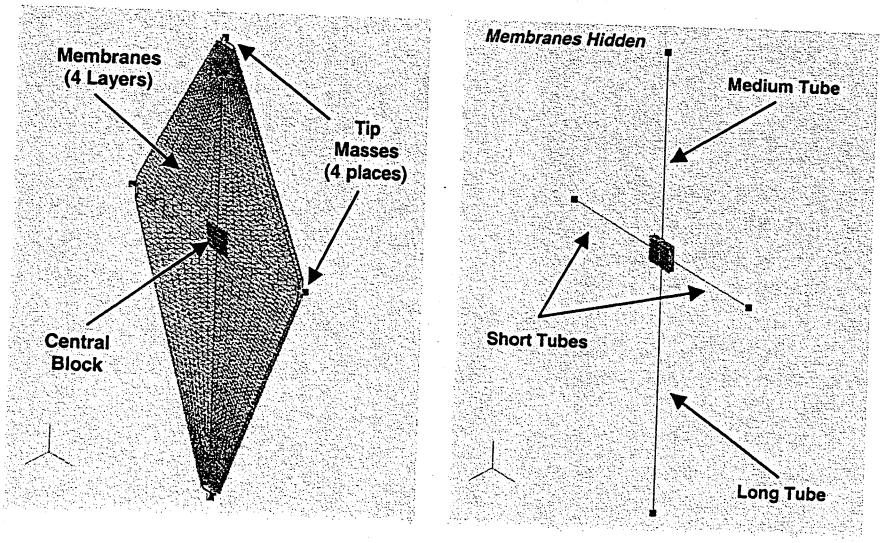

Figure 3: Finite element model of the 1/10th scale model NGST sunshield.

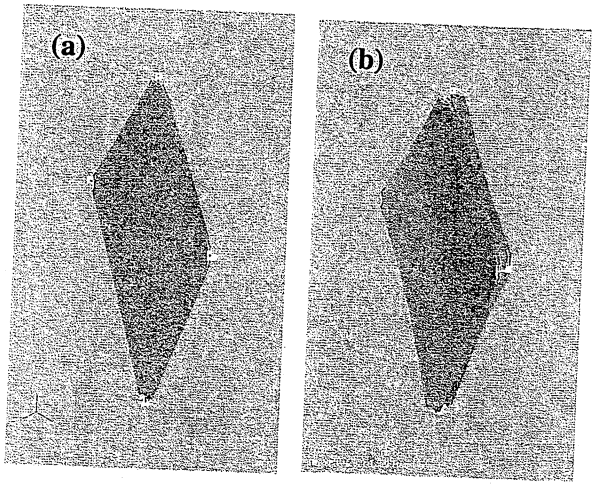

Figure 4: Results from a nonlinear static preloading analysis of the sunshield showing: (a) initially flat and (b) final preloaded configurations (exaggerated).

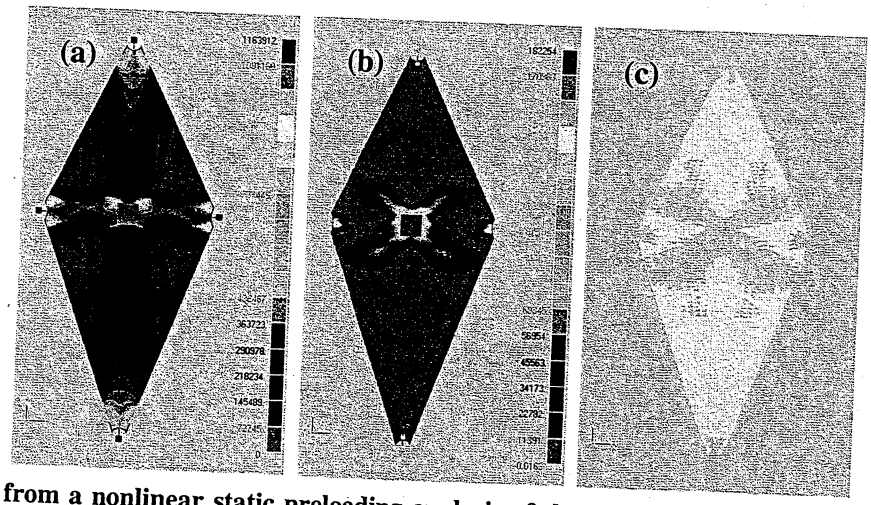

Figure 5: Results from a nonlinear static preloading analysis of the baseline sunshield: (a) major principal stresses, (b) minor principal stresses, and (c) wrinkled region.

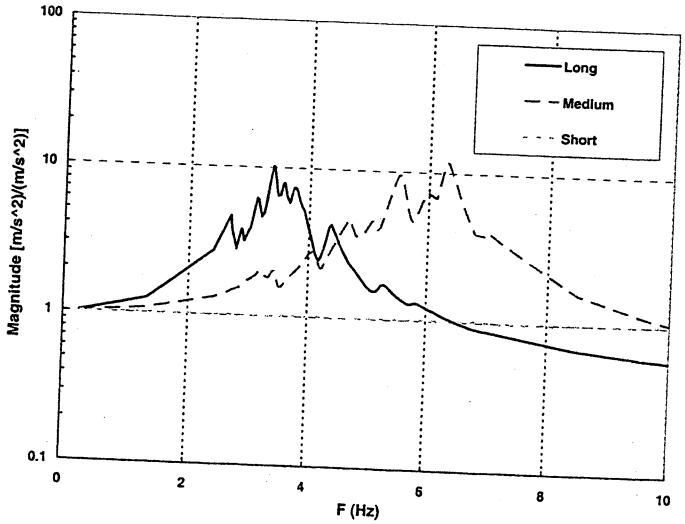

Figure 6: Results from a random response analysis of the baseline sunshield showing acceleration transfer function magnitudes for the tips of the long, medium, and short support tubes.

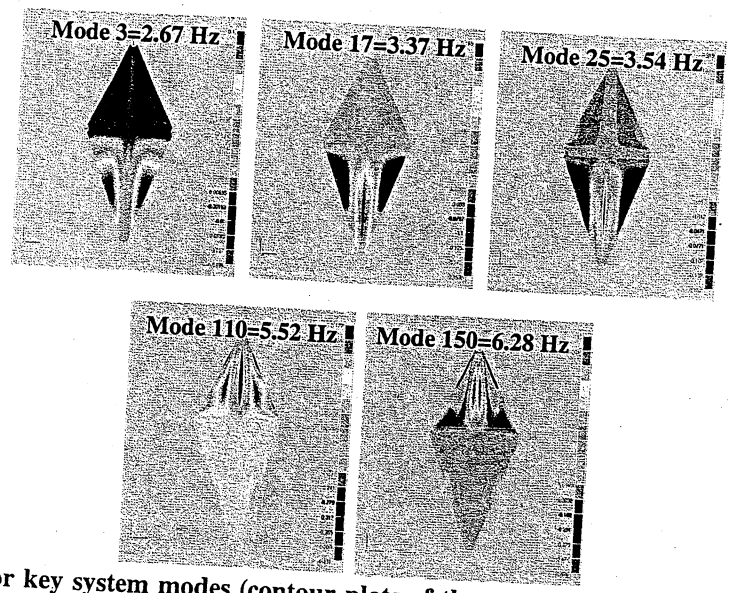

Figure 7: Mode shapes for key system modes (contour plots of the out-of-plane displacements for the outer membrane layer).

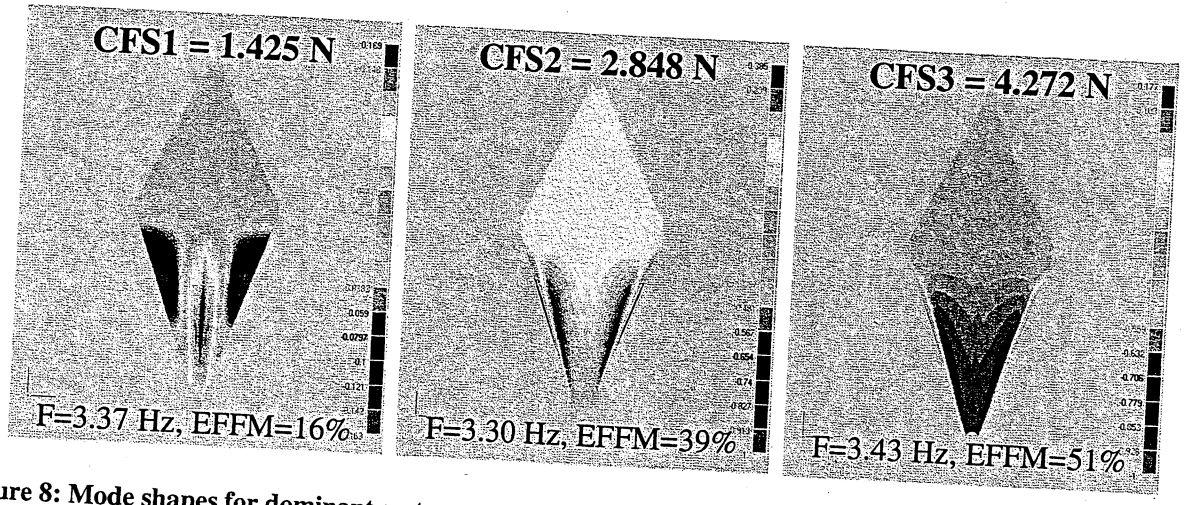

Figure 8: Mode shapes for dominant system mode from preload effects study.

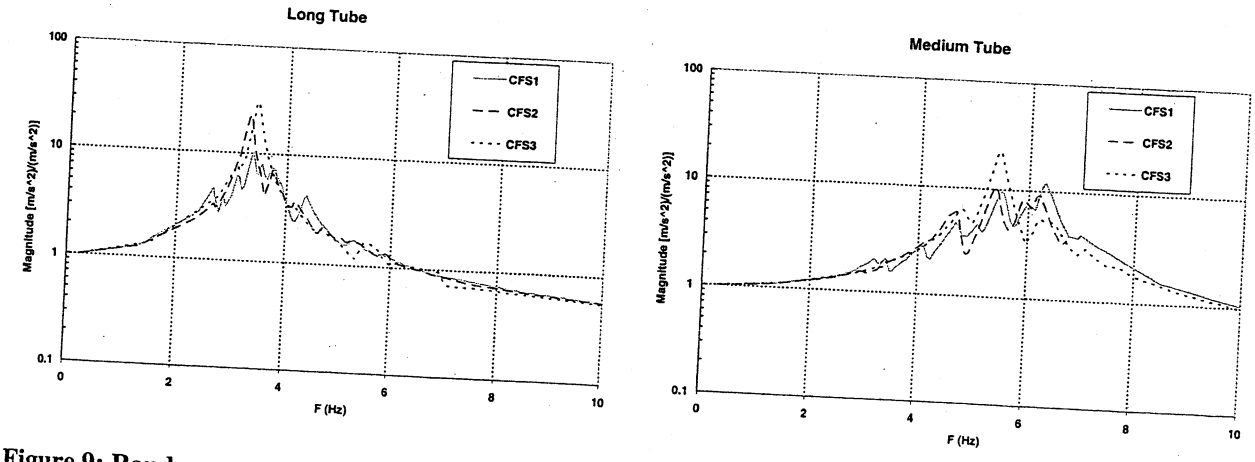

Figure 9: Random response analysis results from preload effects study showing acceleration transfer function magnitudes for the tips of the long and medium support tubes.

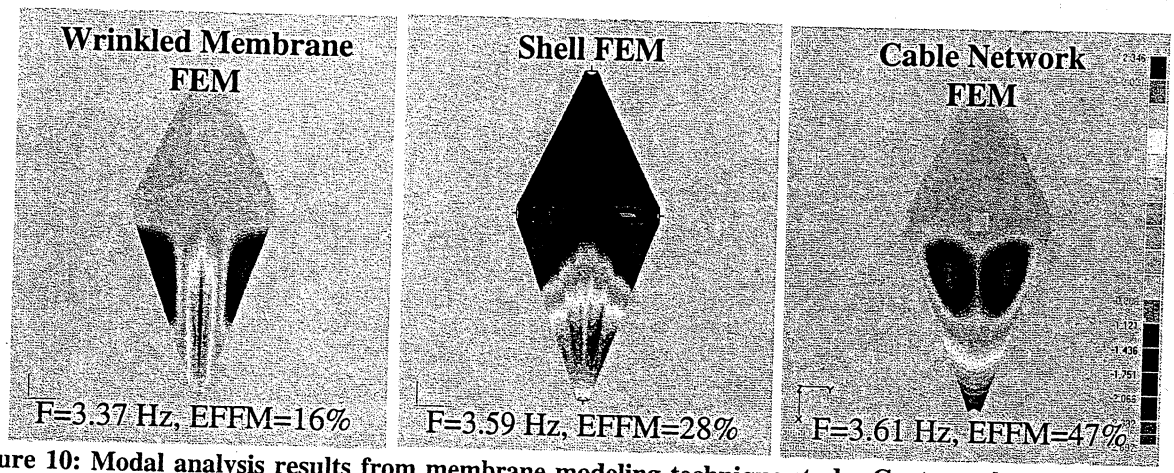

Figure 10: Modal analysis results from membrane modeling technique study. Contour plots of out-of-place displacements of the outer membrane layer for mode B.

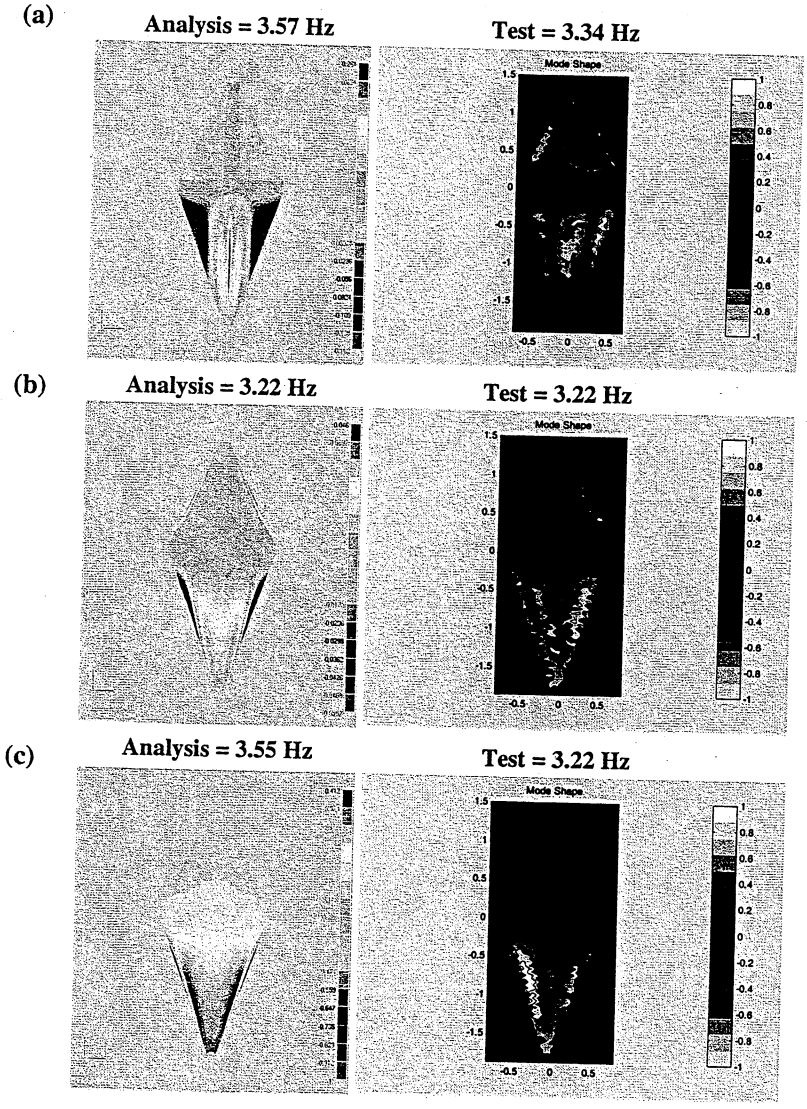

Figure 11: Comparison of analytical predictions and dominant modes from ground tests: (a) CFS1 – long side down orientation, (b) CFS2 – long side down orientation, and (c) CFS3 – long side down orientation.